Meteorologische Zeitschrift, Vol. 23, No. 5, 483–490 (published online April 4, 2014)

A simple dynamical model of cumulus convection for data assimilation research

Michael Würsch[1,2*] and George C. Craig[1,2]

[1]Hans-Ertel-Centre for Weather Research, Data Assimilation Branch, Ludwig-Maximilians-Universität, München, Germany
[2]Meteorologisches Institut, Ludwig-Maximilians-Universität München, Germany

(Manuscript received April 16, 2013; in revised form November 25, 2013; accepted December 23, 2013)

Abstract

A simplified model for cumulus convection has been developed, with the aim of providing a computationally inexpensive, but physically plausible, environment for developing methods for convective-scale data assimilation. Key processes, including gravity waves, conditional instability and precipitation formation, are represented, and parameter values are chosen to reproduce the most important space and time scales of cumulus clouds. The model is shown to reproduce the classic life cycle of an isolated convective storm. When provided with a low amplitude noise source to trigger convection, the model produces a statistically steady state with cloud size and cloud spacing distributions similar to those found in radiative-convective equilibrium simulations using a cloud resolving model. Results are also shown for convection triggered by flow over an orgraphic obstacle, where depending on the wind speed two regimes are found with convection trapped over the mountain, or propagating downstream. The model features prognostic variables for wind and rain that can be used to compute synthetic observations for data assimilation experiments.

Keywords: Data Assimilation, Modelling, Shallow water dynamics

1 Introduction

Numerical weather prediction (NWP) models are currently reaching resolutions on the order of 1 km. At this scale, deep cumulus convection is not parameterized and observations of convective storms should be assimilated in the model analysis. As conventional data do not have the required horizontal and temporal resolution, the use of remote sensing data such as radar will be of primary importance. However these data sources create additional challenges for a data assimilation system (see review by Dance (2004)). The patchy nature of observed precipitation fields can lead to non-Gaussian error distributions dominated by "hit or miss" errors. In addition the rapid development of convective clouds and the nonlinear relationship between observables such as radar reflectivity, and dynamical variables like vertical velocity and water content, lead to large changes in atmospheric state between observation times that are not well approximated by linear dynamics. A notable example is the late detection problem, that occurs because radar cannot detect storms until large precipitation particles have developed, by which time the dynamical circulation is fully developed. Considerable effort is now being expended on developing new algorithms and methods to deal with these challenges (Dance, 2004; Van Leeuwen, 2009; Bocquet et al., 2010).

*Corresponding author: Michael Würsch, Meteorologisches Institut München, Ludwig-Maximilians-Universität, Theresienstr. 37, 80333 München, Germany. e-mail: michael.wuersch@lmu.de

Data assimilation research has benefitted from the availability of a hierarchy of models of varying complexity which can be used to test new methods before implementation in a full NWP system. The use of simple models has two advantages. First, they are generally easier to implement and computationally inexpensive, allowing more extensive testing than would be practical in the full system. Secondly, idealised models isolate particular processes or issues and may be easier to understand and optimise than a more realistic system. In meteorology, much use has been made of a series of simple models introduced by Lorenz (Lorenz, 1963, 1995, 2005), which use a small number of dynamical variables, but capture key aspects of nonlinearity and fast-slow interactions. At a more complex level, the quasi-geostrophic model has proved useful for its more realistic representation of the synoptic-scale structures found in the atmosphere (Ehrendorfer and Errico, 2008).

Unfortunately, models based on low-order dynamical systems or flows close to geostrophic balance do not capture the spatial intermittency associated with the convective scale. As a result, the performance of a data assimilation system in these models may not be representative of its performance in a convective-scale NWP system. The most popular approach to testing convective-scale data assimilation systems is to use an NWP system in an idealised setting. Successful examples have used simulations of idealised storms in a “perfect model” configuration (Snyder and Zhang, 2003; Tong and Xue, 2005; Bischof, 2011; Potvin and Wicker, 2012; Lange, 2013), as well as simplified scenarios based on

DOI 10.1127/0941-2948/2014/0492

real events (Aksoy et al., 2009; Dowell et al., 2011; Dawson et al., 2012). While these experiments have proven very useful, they remain computationally expensive and only a limited number of data assmilation algorithms and configurations have been investigated. Ideally, one would like to have a hierarchy of models designed to represent the dynamics and physics of the atmosphere on the convective scale, and in particular to represent the key processes of cumulus convection itself.

At the opposite extreme of complexity to an NWP system, Craig and Würsch (2013) introduced a simple stochastic model, based on a spatial Poisson birth-death process designed to capture the spatial intermittency and nonlinearity of a developing convective cloud field. Two data assimilation algorithms, the Local Ensemble Transform Kalman Filter (LETKF) of Hunt et al. (2007) and the Sequential Importance Resampling particle filter (Van Leeuwen, 2009), were tested, and some insight was obtained into their characteristic errors. However this very idealised model omits many physical processes that may be relevant for data assmilation. Most importantly, the model has no spatial correlations between dynamical variables, and will not benefit from the ability of an assimilation algorithm to accurately represent background error covariances.

The purpose of this paper is to introduce a convection model of intermediate complexity, with dynamics based on the equations of fluid motion, but substantially less expensive than a NWP model. The model will be designed to represent conditional instability, where the atmosphere is unstable to upward displacements of sufficient magnitude, providing a representation of cloud formation, but stable to smaller or downward displacements, allowing propagation of gravity waves. Additionally the model will include the negative buoyancy effect of rainwater that limits the growth of convective clouds. An important goal of the simple model is that it shows not only a qualitative resemblance to atmospheric convection, but that it accurately represents the key space and time scales of storm development. Being based on fluid equations, a numerical implementation is required, and can be developed using analogous methods to the full equations used in NWP models. Finally, the model will predict variables such as horizontal velocity and rain water concentration, allowing the computation of synthetic observations analogous to Doppler winds and radar reflectivity for data assimilation experiments.

The paper is organized as follows: In Section 2 the model equations are developed and parameter values leading to physically reasonable behavior are proposed. The numerical implementation and design of the simulation experiments is also discussed. Section 3 examines the behavior of the idealised model, considering the life cycle of a typical cloud, the properties of an ensemble of clouds in a statistically steady state, and regimes of behavior for orographically triggered convection. The performance of the model is summarised in Section 4. A future paper will describe some initial experiments applying the LETKF to this system.

2 Model description

The mass and temperature perturbations that cumulus clouds introduce into their environment are communicated in space by radiation of gravity waves. Neighbouring clouds may be initiated or enhanced by uplift, or suppressed by downward motion associated with the waves. The primary importance of gravity waves suggests a model based on the shallow water equations:

$$\frac{\partial u}{\partial t} + u\frac{\partial u}{\partial x} + \frac{\partial \phi}{\partial x} = K\frac{\partial^2 u}{\partial x^2}, \tag{2.1}$$

$$\frac{\partial h}{\partial t} + \frac{\partial (uh)}{\partial x} = K\frac{\partial^2 h}{\partial x^2}, \tag{2.2}$$

where u is the fluid velocity, h the depth of the fluid, H the height of the topography which will be used later, and the geopotential $\phi = g(H+h)$ is the absolute fluid layer height $(H+h) = Z$ multiplied by the gravitational acceleration g. A diffusion term with constant K has been included in both equations. If the initial absolute fluid layer height is H_0, the gravity wave speed is given by $c = (g \cdot H_0)^{1/2}$.

To provide a representation of cumulus convection, the shallow water equations must be extended to include conditional instability, i.e. positive buoyancy due to latent heat release in ascending, saturated air. This will be accomplished by modifying the geopotential ϕ. The standard definition of ϕ is based on the height of the fluid surface, and its gradient provides a momentum forcing away from regions of increased surface height. This will be altered when the height exceeds a threshold H_c, representing the level of free convection. At these positions, the geopotential is replaced by a relatively low constant value ϕ_c, as illustrated in Fig. 1.

The gradient of geopotential will thus force fluid into the region of decreased geopotential, increasing the fluid depth there. Once such a "cloud" forms, the width of the region with altered geopotential will expand until limited by diffusion, as occurs for cumulus clouds in simulations with kilometre-scale weather prediction models.

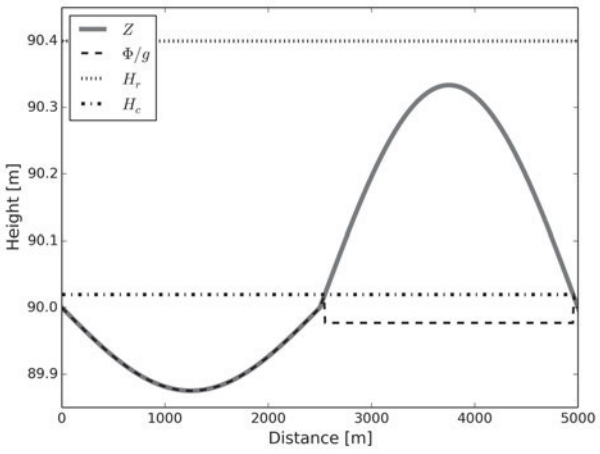

Figure 1: Sketch showing the modification of the geopotential ϕ in a cloud which is still below the rain threshold.

The realistic world equivalence of a cloud in our model would be an updraft or the production of rain water. As the modified shallow water model does not distinguish between these processes, it will be called cloud as long as the water level is above the threshold, even when the movement is downward. When a cloud is formed, the fluid level would continue to rise until the height gradient becomes so strong that diffusion prevents further gowth. This is less realistic, because in nature the lifetime of a cumulus cloud in an unsheared environment is limited by the formation of heavy precipitation particles that eventually overcome the postive buoyancy and turn the updraft into a downdraft. This effect will be mimicked by introducing a new variable r. It is just the mass fraction of rain water and multiplied by c^2 can be added to the geopotential. A separate conservation equation for r is then added, with the following source and sink terms. Rainwater is produced when the fluid level exceeds a threshold value H_r, and is rising (u has positive convergence). The rain production threshold is set higher than the threshold for buoyancy to ensure that rain production is delayed relative to the onset of the cloud circulation. Removal of rain by precipitation is modelled by a simple linear relaxation towards zero.

The modified shallow water equations are:

$$\frac{\partial u}{\partial t} + u\frac{\partial u}{\partial x} + \frac{\partial(\phi + c^2 r)}{\partial x} = K\frac{\partial^2 u}{\partial x^2} + F, \tag{2.3}$$

where

$$\phi = \begin{cases} \phi_c + gH, & Z > H_c \\ g(H+h), & \text{otherwise.} \end{cases} \tag{2.4}$$

A forcing term F has been added to the momentum equation and will be discussed further in Section 2.2. The continuity equation reads

$$\frac{\partial h}{\partial t} + \frac{\partial(uh)}{\partial x} = K\frac{\partial^2 h}{\partial x^2}, \tag{2.5}$$

and the equation for rain water is given by

$$\frac{\partial r}{\partial t} + u\frac{\partial r}{\partial x} = K_r\frac{\partial^2 r}{\partial x^2} - \alpha r - \begin{cases} \beta\frac{\partial u}{\partial x}, & Z > H_r \text{ and } \frac{\partial u}{\partial x} < 0 \\ 0, & \text{otherwise,} \end{cases} \tag{2.6}$$

where α and β are constants discussed below. Note that the equations are written for a single horizontal dimension x, but could be trivially extended to two horizontal dimensions. Coriolis force could also be taken into account but will only have an effect on larger scales which are not considered here.

2.1 Parameter selection

Values for the physical parameters are chosen to produce realistic space and time scales for the model clouds, as explained in the following list.

- $H_0 = 90\,\text{m}$ is chosen to give a gravity wave speed of 30 m/s, typical for the gravest internal mode in the troposphere (Gill, 1982).
- $H_c = 90.02\,\text{m}$ and $\phi_c = 899.77\,\text{m}^2\text{s}^{-2}$ give a reasonable cloud fraction of roughly five percent, and a time for the cloud to develop to full height of about half an hour.
- $H_r = 90.4\,\text{m}$ and $\beta = 1/300$ imply a lag between cloud and rain formation of about 15 min, and a cloud lifetime of about 1–2 hr.
- $\alpha = 2.5 \cdot 10^{-4}\,\text{s}^{-1}$ corresponds to a half-life for the influence of rain of roughly 1 hr. This gives persistence of rain and associated negative buoyancy even after the collapse of the height perturbation.

Note that these choices of parameter values are not unique. For example, the time between initiation of a cloud and first rain can be influenced by changing H_r, H_c or ϕ_c. The values of K and K_r are chosen mainly for numerical smoothness and depend on the resolution of the discretized equations but also have an important effect on the size of the clouds which will be discussed later. These aspects are discussed in Section 2.3 below.

2.2 Initiation of convection

Convective clouds in nature are initiated by low-level disturbances that rise boundary layer air to its level of free convection. The modified shallow water model presented here also requires a trigger mechanism to initiate convection. We explicitly consider two processes: perturbations originating below cloud base associated with the convective boundary layer, and flow over orographic obstacles. In addition, secondary initiation by existing storms can also trigger clouds. It will be shown later that gravity waves radiating from convective clouds can provide sufficient lifting to initiate new convection even in the simple model. Another secondary initiation mechanism, lifting of air over cold pools generated by evaporation of precipitation, will not be considered.

Convective clouds are often triggered by buoyant plumes in the dry convective boundary layer beneath the cloud layer which provide vertical displacements that can initiate convective updrafts. This process can be modeled by adding random convergent wind perturbations that elevate the fluid surface. In particular, perturbations F_n of the form

$$F_n = \bar{u}\frac{\partial}{\partial x}\left(e^{-(x-x_n)^2/l^2}\right), \tag{2.7}$$

are added to u, with amplitude $\bar{u}$, length scale l, centered at location x_n. In the simulations that use this method of convective initiation, perturbations are added each timestep at a random number of locations with random positions. For the results presented in this work, $l = 2000\,\text{m}$, and $\bar{u} = 0.005\ \text{ms}^{-1}$. The length scale is related to the size of boundary layer eddies, which in nature scales with the depth of the subcloud layer, about 1 km. Perturbations are added at random locations x_n at a rate of $1.6 \times 10^{-6}\,\text{m}^{-1}\text{s}^{-1}$, which corresponds to approximately one perturbation in a 1 km region every

10 minutes (a typical eddy turnover time for the convective boundary layer).

Examples of the initiation of convection by orography will be presented in Section 4.

2.3 Numerical implementation

The numerical implementation of the shallow-water equations follows Gohm and Mayr (2004), based on previous work by Schär and Smith (1993a,b). The equations are discretized by standard second-order centered differences on a staggered grid. A RAW Filter (Williams, 2009, 2011) is used for time-smoothing of all model variables. For the simulations shown in this paper, the domain size L is 500 km, the horizontal resolution $dx = 500$ m, and the time step $dt = 5$ s, and the diffusion constant $K = 25000\,\mathrm{m^2\,s^{-1}}$ for h and u and a smaller $K_r = 200\,\mathrm{m^2\,s^{-1}}$ for the rain variable. As with models that simulate convection by solving the full equations of motion with kilometre-scale resolution, the resolution and diffusion control the size of the model clouds. As a result, the values of the physical parameters identified in Section 2.1 might have to be reconsidered if a different numerical implementation or resolution were used. While this resolution dependance is not ideal, similar behaviour is also found in numerical weather prediction models where convective properties change significantly with resolution (Bryan and Morrison, 2011).

3 Randomly triggered convection

As a first example, results will be shown for convection triggered at random in space and time by boundary layer disturbances. In these experiments no mean wind is imposed and no orography is present. The model is initiated with a constant surface at 90 m. The triggering disturbances are as described in Section 2.2, and lead to a statistically steady ensemble of clouds throughout the domain. The background noise starts with the first time step and stays active for the whole simulation. The results should be comparable to radiative-convective equilibrium simulations of convection (Tompkins and Craig, 1998; Cohen and Craig, 2006) produced with a cloud resolving model. First, the life cycle of a single cloud within the simulation is considered and after that the cloud size distribution and a measure of clustering are presented.

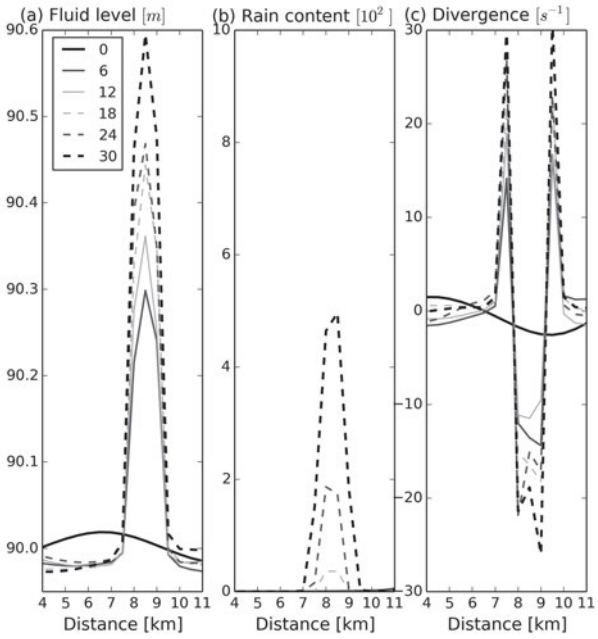

Figure 2: Updraft phase of a cloud. The different lines correspond to different times in minutes.

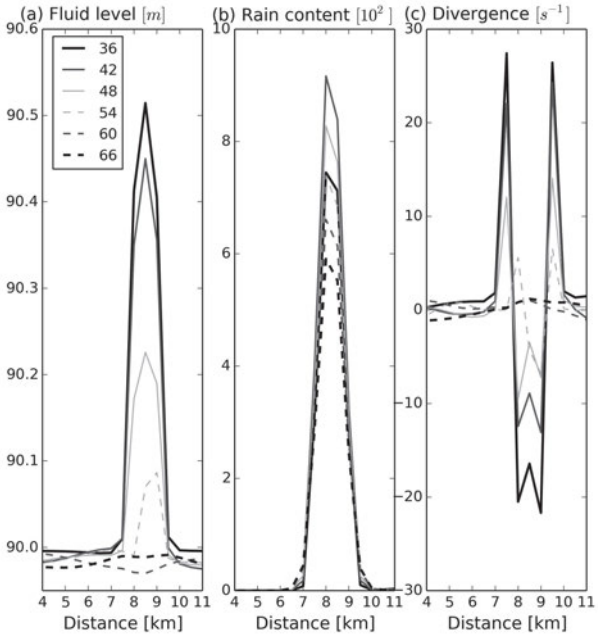

Figure 3: Downdraft phase of a cloud. The different lines correspond to different times in minutes.

3.1 Life cycle of a convective cloud

Figs 2 and 3 show an example of the temporal evolution of the fluid level, rain content and divergence fields in a typical convective cloud. The plots focus on a small subdomain of 14 grid points (7 km) and each line corresponds to a different time with the interval being 6 minutes. In Fig. 2 one can see the building and strengthening of an updraft. At time 0 there is just a small positive perturbation in the fluid level. This initial peak may have come from the background perturbations or the influence of neighboring updrafts. Since this peak reaches above H_c, the modifed geopotential causes fluid to flow into the updraft of the cloud region and the fluid level continues to rise.

The divergence plot shows a steady convergence into the cloud, with sharp positive divergence peaks on both sides of the updraft. It also shows that the convergence was already located a little bit to the right of the fluid maximum at time 0. Rain starts to accumulate after

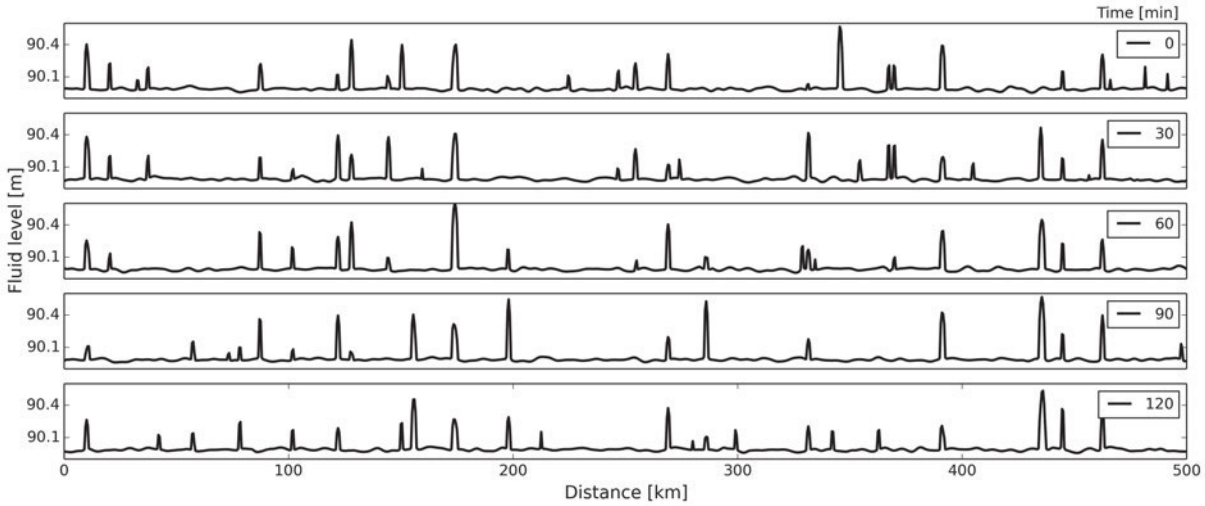

Figure 4: Typical evolution of the cloud field in the whole model domain.

about 15 minutes when the fluid level reaches above 90.4 m and is still converging. In this example cloud, the downward force associated with the rain becomes strong enough to prevent further increase in the fluid level after about 30 minutes, although the accumulated rain maximum is not reached until minute 42. After another 30 minutes the height perturbation has collapsed leaving gravity wave perturbations that propagate away. The weakening of the convergence zone during the collapse of the cloud is clearly visible in Fig. 3c. As there is still a significant amount of rain present at 60 minutes, this location is unfavourable for convection for some time afterwards. This effect is the reason why the half-life of rain was chosen to be 1 hour instead of the 10 to 15 minutes rain stays in the real atmosphere, and attempts to describe the modification of the subcloud layer by rain which inhibits convection.

A view of the ensemble of clouds over the full 500 km domain is shown in Fig. 4.

The fluid level is displayed at 30 minute intervals over a period of 2 hours. There is a wide range of different sized clouds with different life cycles visible. Some last for a short time while others persist throughout the period.

In addition to the simple life cycle illustrated in Figs 2 and 3, another typical cloud behaviour occurs when the rain starts to push down the fluid level. This happens when the rain does not manage to completely kill the updraft. When the water level is getting pushed down and between the two thresholds, the upward forcing is still active. During this phase rain is also being removed. If too much rain is removed, the upward forcing will be stronger again and the cloud gets pushed upward again. This is visible for example in the first cloud from the left or the cloud around kilometre 130 in Fig. 4 which still exists after 2 hours. In such cases clouds can undergo multiple phases of growth and decay until they are finally destroyed either by the rain, the background perturbations or the influence of gravity waves emitted from other clouds.

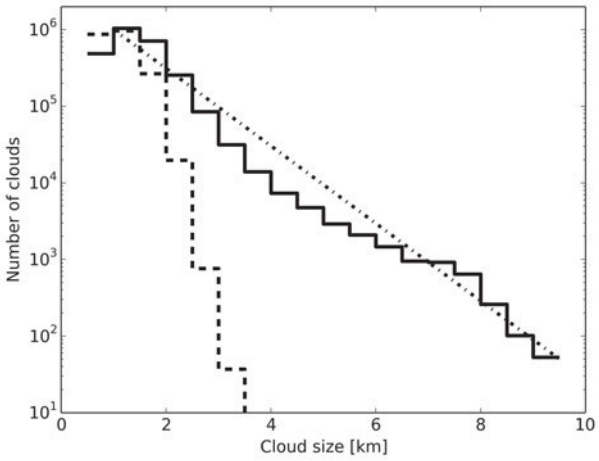

Figure 5: Logarithmic cloud size distribution for all clouds with a height above 90.04 (solid) and clouds which do not precipitate (dashed).

The number and location of clouds in the domain will be determined by a combination of effects: triggering of clouds by the imposed wind perturbations or upward displacements associated with gravity waves, and suppression by downward gravity wave displacements or negative buoyancy due to rain that remains from an earlier cloud. The effect of these processes on the spatial distribution of clouds will be seen in the next section.

3.2 Statistics of convection

Statistics of the size and relative location of clouds have been calculated using output every 30 minutes for a long model integration (almost 10 years). Figure 5 shows a logarithmic histogram of the cloud size where a cloud is defined as a region where $Z > 90.04$ m. This threshold is chosen so the smallest perturbations around $H_c = 90.02$ m are not identified as a cloud. The distribution approximately matches the exponential form (dash-dotted black line) expected from theory (Craig and Cohen, 2006) and obtained in cloud resolving models in

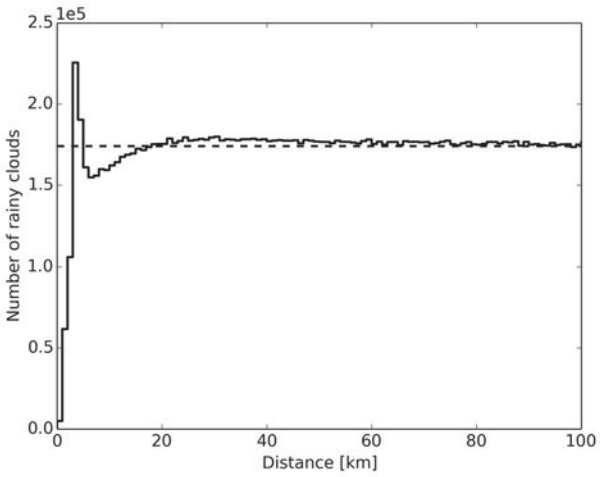

Figure 6: Distribution of distance between different clouds.

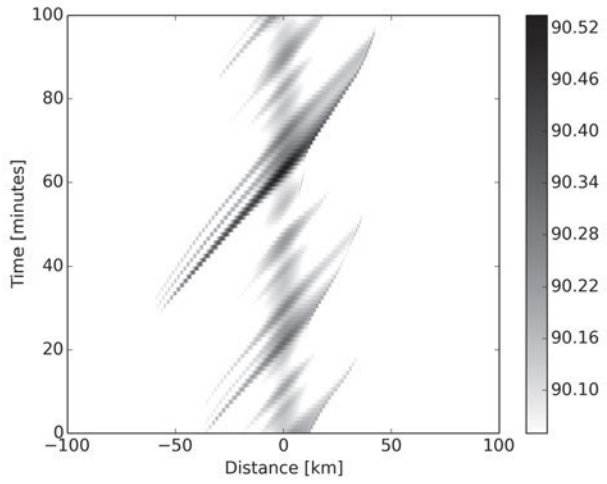

Figure 7: Hovmöller diagram for a mean wind of $30\,\mathrm{ms}^{-1}$. Marked are only gridpoints where the water level is above 90.05 m. Distance 0 coincides with the mountain peak.

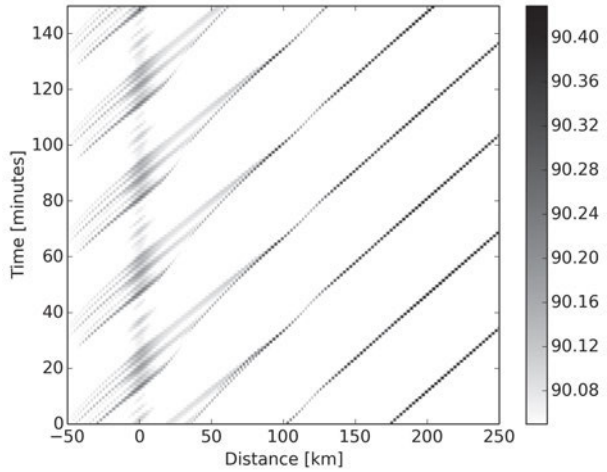

Figure 8: Same as Fig. 7 with a mean wind of $40\,\mathrm{ms}^{-1}$.

a radiative-convective equilibrium (e.g. Figure 2 of Cohen and Craig (2006)).

The average size is 1.7 km, with the most common value being about 1 km and values over 8 km being very rare. The average number of clouds present in the domain at a given time is 14.9, which leads to an average convective area fraction of about 5 % of the domain. As can be seen in the dashed line of Fig. 5, the clouds without rain all have sizes between 1 and 3.5 km. This distribution is very steep and decreases from almost 10^6 to 10 in this range. Therefore almost all of the larger clouds produce precipitation.

In Fig. 6 is a histogram of the distance between pairs of clouds. The dashed line indicates the uniform distribution that would be expected if the positions of the clouds were completely uncorrelated (a spatial Poisson process).

Cloud separations of less than 3 km are uncommon since this is below the average width of the individual clouds, however there is a pronounced peak in the distribution at a distance of approximately 3.5 km, which appears to be associated with strong gravity wave perturbations initiating new clouds near existing ones. Separation distances of 6 to 18 km are less common, reflecting a suppression of convection due to reduced average fluid levels in the vicinity of a cloud. At long distances the separation frequency approaches the value expected for uncorrelated cloud locations. This pattern of enhanced frequency of clouds at very short separations, with a region of reduced frequency at somewhat larger distances, is also found in Figures 6a and 8a of Cohen and Craig (2006).

4 Orographically triggered convection

In this section, results are presented for convection triggered by flow over a bell shaped mountain with a half-width of 10 km and a height of 0.2 m. No random perturbations are used, but a mean wind is introduced. For sufficiently large wind speeds the resulting flow can displace the fluid level above H_c and initiate a cloud. The orography and the mean wind pose problems for the numerics and it was found necessary to reduce the time step to 1 s and increase the diffusion to $30000\,\mathrm{m}^2\,\mathrm{s}^{-1}$.

Results for two values of mean wind speed are shown in the form of space-time (Hovmöller) plots indicating where fluid depth exceeds 90.05 m. With a mean wind of $30\,\mathrm{ms}^{-1}$, clouds are present over the mountain at all times, growing on the upwind side and decaying downwind. Sometimes clouds or small clusters of clouds are initiated some distance upwind of the mountain by gravity waves (Fig. 7). A different behaviour occurs for wind speeds larger than the intrinsic gravity wave speed of the fluid. For a mean wind of $40\,\mathrm{ms}^{-1}$ (Fig. 8) clouds are no longer initiated upstream, but always over the mountain. Most decay on the downwind side, but some are advected downstream away from the mountain. These interact and merge, eventually leading to a sequence of propagating convective storms with a sepa-

ration distance of roughly 75 km, moving at a speed of about 35 ms^{-1}.

These two regimes compare favorably with simulations of flow over a ridge by Chu and Lin (2000). The behaviour for a windspeed of 30 ms^{-1} is comparable to the quasi-stationary convective system in regime (II) of Chu and Lin (2000), with cells developing on the upstream side of the ridge and decaying on the downstream side. The results for a windspeed of 40 ms^{-1} correspond to regime (III) with quasi-stationary and downstream propagating systems. It should be noted however that the simple model presented here does not produce the full range of behaviours described by Chu and Lin (2000) or the more recent study of Miglietta and Rotunno (2009), which involve complex interactions with evaporation-driven cold pools that are not represented in the modified shallow water model.

5 Conclusions

A simplified dynamical model which is designed to represent key features of cumulus convection has been presented. The model is based on the shallow water equations and allows propagation of gravity waves. Conditional instability is represented by modifying the geopotential to produce convergence when the fluid level exceeds a height threshold. A rain variable is introduced that provides a downward force that can lead to the destruction of a cloud.

Two mechanisms for initiation of convection have been considered. The first is a stochastic noise term representing subcloud layer disturbances, and the second flow over an orgraphic obstacle. With a continuous stochastic forcing, the model produces an ensemble of clouds that is comparable to radiative-convective equilibrium simulations using more sophisticated models. In particular, the clouds undergo a realistic life cycle with a rapid intensification, formation of precipitation, followed by collapse. The cloud size distribution roughly corresponds to the exponential form predicted by Craig and Cohen (2006), and the cloud spacing shows the effects of local triggering and more distant suppression of convection by gravity waves. With orographic triggering, two regimes of convection are found, depending on the background wind speed. With wind speeds up to the intrinsic gravity wave speed, convection is trapped over the orography, while for larger wind speeds, clouds develop over the orography but periodically move downstream.

While the simple model reproduces many behaviours of real convection, some aspects are excluded. First the model is assumed to be one dimensional. A two dimensional version could easily be constructed, although the choices of parameter values would need to be reexamined. Secondly the interaction of convection with synoptic or larger scales in the atmosphere is not represented. The use of constant values for H_c and ϕ_c implies that the conditional instability of the atmosphere is uniform in space and time. In principle these variables could be coupled to the dynamical equations, but many details would need to be addressed. The absence of a representation of convective feedbacks on the subcloud layer, most importantly the creation and interaction with cold pools, implies that the simple model will not produce important modes of mesoscale convective organisation, such as squall lines. Adding such a representation is not trivial and would probably require the introduction of one or more prognostic variables.

The aim of this work was to provide a contribution to a hierarchy of convection models for data assimilation research, that sits between the very simple stochastic model of Craig and Würsch (2013), and the full solution of the fluid equations in kilometre-scale weather prediction models. In contrast to the model of Craig and Würsch (2013) which ignored interactions between convective clouds, the present model includes gravity waves, allowing initiation and inhibition effects, leading to a realistic spatial distribution of clouds (Section 3.2). The availability of wind and rain variables that correspond to physically observable quantities should make it possible to define background and observation error covariance matrices that have similar properties to those arising in full NWP systems. A first examination of the behaviour of a local ensemble transformed Kalman filter using the modified shallow water model is in progress, and results will be presented in a future paper.

6 Acknowledgements

This research was funded by LMU Munich and carried out in the Hans Ertel Centre for Weather Research. This research network of Universities, Research Institutes and the Deutscher Wetterdienst is funded by the BMVBS (Federal Ministry of Transport, Building and Urban Development).

References

Aksoy, A., D.C. Dowell, C. Snyder, 2009: A multicase comparative assessment of the ensemble kalman filter for assimilation of radar observations. part I: Storm-scale analyses. – Mon. Wea. Rev. **137**, 1805–1824.

Bischof, M., 2011: Ensemble Simulations of Convective Storms. – Master's thesis, ETH Zürich.

Bocquet, M., C.A. Pires, L. Wu, 2010: Beyond Gaussian Statistical Modeling in Geophysical Data Assimilation. – Mon. Wea. Rev. **138**, 2997–3023.

Bryan, G.H., H. Morrison, 2011: Sensitivity of a Simulated Squall Line to Horizontal Resolution and Parameterization of Microphysics. – Mon. Wea. Rev. **140**, 202–225.

Chu, C.-M., Y.-L. Lin, 2000: Effects of Orography on the Generation and Propagation of Mesoscale Convective Systems in a Two-Dimensional Conditionally Unstable Flow. – J. Atmos. Sci. **57**, 3817–3837.

Cohen, B.G., G.C. Craig, 2006: Fluctuations in an equilibrium convective ensemble. Part II: Numerical experiments. – J. Atmos. Sci. **63**, 2005–2015.

Craig, G.C., B. G. Cohen, 2006: Fluctuations in an equilibrium convective ensemble. Part I: Theoretical formulation. – J. Atmos. Sci. **63**, 1996–2004.

Craig, G.C., M. Würsch, 2013: The impact of localization and observation averaging for convective-scale data assimilation in a simple stochastic model. – Quart. J. Roy. Meteor. Soc. **139**, 515–523.

Dance, S., 2004: Issues in high resolution limited area data assimilation for quantitative precipitation forecasting. – Physica D: Nonlinear Phenomena **196**, 1–27.

Dawson, D.T., L.J. Wicker, E. R. Mansell, R. L. Tanamachi, 2012: Impact of the Environmental Low-Level Wind Profile on Ensemble Forecasts of the 4 May 2007 Greensburg, Kansas, Tornadic Storm and Associated Mesocyclones. – Mon. Wea. Rev. **140**, 696–716.

Dowell, D., L. Wicker, C. Snyder, 2011: Ensemble Kalman Filter Assimilation of Radar Observations of the 8 May 2003 Oklahoma City Supercell: Influences of Reflectivity Observations on Storm-Scale Analyses. – Mon. Wea. Rev. **139**, 272–294.

Ehrendorfer, M., R. Errico, 2008: An atmospheric model of intermediate complexity for data assimilation studies. – Quart. J. Roy. Meteor. Soc. **134**, 1717–1732.

Gill, A., 1982: Atmosphere-Ocean Dynamics. – International Geophysics Series, Academic Press.

Gohm, A., G.J. Mayr, 2004: Hydraulic aspects of föhn winds in an alpine valley. – Quart. J. Roy. Meteor. Soc. **130**, 449–480.

Hunt, B.R., E.J. Kostelich, I. Szunyogh, 2007: Efficient data assimilation for spatiotemporal chaos: A local ensemble transform kalman filter. – Physica D **230**, 112–126.

Lange, H., 2013: Data assimilation of severe convection using a Local Ensemble Kalman Filter. – Master's thesis, LMU München.

Lorenz, E., 1963: Deterministic nonperiodic flow. – J. Atmos. Sci. **20**, 130–141.

Lorenz, E.N., 1995: Predictability: A problem partly solved. – In: Proc. Sem. Predictability **1**, 1–18.

Lorenz, E.N., 2005: Designing chaotic models. – J. Atmos. Sci. **62**, 1574–1587.

Miglietta, M.M., R. Rotunno, 2009: Numerical Simulations of Conditionally Unstable Flows over a Mountain Ridge. – J. Atmos. Sci. **66**, 1865–1885.

Potvin, C.K., L.J. Wicker, 2012: Comparison between Dual-Doppler and EnKF Storm-Scale Wind Analyses: Observing System Simulation Experiments with a Supercell Thunderstorm. – Mon. Wea. Rev. **140**, 3972–3991.

Schär, C., R. Smith, 1993a: Shallow-water flow past isolated topography. Part I: Vorticity production and wake formation. – J. Atmos. Sci. **50**, 1373–1400.

Schär, C., R. Smith, 1993b: Shallow-water flow past isolated topography. Part II: Transition to vortex shedding. – J. Atmos. Sci. **50**, 1401–1412.

Snyder, C., F. Zhang, 2003: Assimilation of Simulated Doppler Radar Observations with an Ensemble Kalman Filter. – Mon. Wea. Rev. **131**, 1663–1677.

Tompkins, A.M., G.C. Craig, 1998: Radiative-convective equilibrium in a three-dimensional cloud-ensemble model. – Quart. J. Roy. Meteor. Soc. **124**, 2073–2097.

Tong, M., M. Xue, 2005: Ensemble Kalman Filter Assimilation of Doppler Radar Data with a Compressible Nonhydrostatic Model: OSS Experiments. – Mon. Wea. Rev. **133**, 1789–1807.

Van Leeuwen, P.J., 2009: Particle filtering in geophysical systems. – Mon. Wea. Rev. **137**, 4089–4114.

Williams, P.D., 2009: A proposed modification to the Robert-Asselin time filter. – Mon. Weather Rev. **137**, 2538–2546.

Williams, P.D., 2011: The RAW Filter: An Improvement to the Robert-Asselin Filter in Semi-Implicit Integrations. – Mon. Wea. Rev. **139**, 1996–2007.